An efficient fatigue assessment model of offshore wind turbine using a half coupling analysis

Chaoshuai Han[a,*], Changguan Mo[a], Longbin Tao[a,b], Yongliang Ma[c], Xu Bai[a]

[a]School of Naval Architecture and Ocean Engineering, Jiangsu University of Science and Technology, Zhenjiang, Jiangsu, PR China

[b]Department of Naval Architecture, Ocean & Marine Engineering, University of Strathclyde, Glasgow G4 0LZ, United Kingdom

[c]School of Shipping and Navy Architecture, Chongqing Jiaotong University, Chongqing, PR China

Abstract

Fatigue failure is an important issue for offshore wind turbine support structures. Especially, fully coupled time domain analysis will lead to high computational burden. Therefore, accurate and efficient fatigue evaluation methods have always been the common goal pursued by the industry and researchers. This paper evaluates fatigue damage under combined wind and wave loading, using a fixed jacket offshore wind turbine as an example. A half coupling model (HCM) with distinct advantage by considering aerodynamic damping and structural damping is developed for dynamic response analysis of offshore wind turbine. The precision and effectiveness of the developed HCM is verified to be reasonable by comparing with numerical simulated

* Corresponding author.

E-mail address: hanchaoshuai@hrbeu.edu.cn

results. A linearized Morison equation is proposed to achieve frequency domain analysis of wave response which is embedded as a programming module in ANSYS. Based on the developed model, dynamic response analysis is carried out under wind and wave loading, and then combined stress spectra at the location of different tubular joints (X-joint and K-joint) are obtained. To consider the interaction of wind and wave, a spectral fatigue combination rule based on Han and Ma's method is used to calculate fatigue damage. The developed combination rule is assessed by compared with time domain fatigue result based on rainflow cycle counting. Analysis using the newly developed model and method demonstrates a high accuracy and efficiency for fatigue damage prediction.

Keywords: Fatigue damage assessment; Offshore wind turbine; Half coupling model; A linearized Morison equation; A spectral combination rule

1 Introduction

In recent years, with increasing concern over the issue of climate change, rapid development of offshore wind energy has been witnessed around the world. In particular, offshore wind energy has huge growth potential in the Asian region which has the opportunity to become the region with the largest installed scale of offshore wind power, thereby significantly promoting the development and utilization of global renewable energy [1-3].

Support structures are very important parts of offshore wind turbines (OWTs) and of great significance to ensure the service life. The support structures are mostly

composed of steel pipes. The tubular connections are prone to stress concentration because of complex structural shape, welding and discontinuous intersection parts. In addition, during the operation, support structures of OWT generally suffer the cyclic load due to turbulent wind and random wave during the service life [4-5]. Hence, fatigue problems have become the control link of design and safety assessment of OWTs. A reasonable and reliable structural fatigue life prediction method is particularly important for the overall structural safety assessment of offshore wind turbines.

At present, Non-linear fully coupling fatigue analysis method is still accurate as a standard in the industry [6]. Based on these studies, some integrated coupling analysis and design tools are developed such as FAST, HAWC2, USFOS, DUWECS. Koukoura et al. [7] investigated the effect of damping on the side–side fatigue based on an integrated coupling model of offshore wind turbine with the aero-hydro-servo-elastic code. Marino et al. [8] studied fatigue loads of a bottom-supported offshore wind turbine under different wind conditions and for different wave modelling assumptions based on the coupled hydro-aero-elastic model. Rezaei et al. [9] investigated the fatigue life sensitivity of a reference 5MW wind turbine under operational and non-operational conditions using coupled time-domain finite element simulations. Li et al. [10] studied short-term fatigue damage at the tower base of a 5 MW FOWT with a spar-type platform with fully coupled time-domain simulations code FAST. Kvittem et al. [11] performed long term time domain analysis of the nominal stress for fatigue assessment of the tower and

platform members of a three-column semi-submersible by fully coupled time domain analyses in Simo-Riflex-AeroDyn. Yang et al. [12] investigates the wind-wave coupling effects on fatigue damage of tendons that connect multiple bodies of a novel floating platform (TELWIND) supporting a 10 MW wind turbine with an aero-hydro-servo tool.

Non-linear fully coupling time domain simulation approach can potentially lead to more reliable design solutions for fatigue assessment of OWT [13-17]. The high computational effort is required since a large number of environmental states and load cases need to be considered when calculating the fatigue life of OWT support structures [18]. For example, fatigue analysis of an OWT project in Block Island produced 25 cases and 2334 time domain simulations. The calculation lasted 10 days using 5 workstations with 24-core.

In order to improve the efficiency of coupling analysis, many researchers concentrated on developing decoupling or half coupled models to conduct fatigue analyses. Chen et al. [19] developed a computationally efficient methodology combining aerodynamic decoupling and modal reduction techniques for fatigue life prediction. Sun et al. [20] established an analytical model of an offshore wind turbine coupled with a 3D-PTMD (full description of PTMD upon first appearance) using the Euler-Lagrangian equation. Yeter et al. [14, 21] dealt with the evaluation of the spectral fatigue damage prediction of a tripod offshore wind turbine support structure subjected to combined stochastic wave and wind-induced loads using spectral fatigue

analysis method. Li et al. [22] proposed a probabilistic long-term fatigue damage assessment approach to reduce the calculation cost for this time-consuming process by implementing a C-vine copula model and a surrogate model. Lin et al. [23] proposed a methodology to develop reduced-order models to support the operation and maintenance of offshore wind turbines.

As the wind turbine size increases, it is questionable whether this de-coupled analysis method yields sufficiently accurate results. Wang et al. [24] conducted a comparative study of the drivetrain dynamic behaviour obtained by a fully coupled method and a de-coupled one for a 10-MW floating wind turbine. This study showed that the de-coupled method could provide accurate results in the drivetrain fatigue damage. Therefore, by using a de-coupled approach, fatigue damage can be not only assessed very quickly, but also without loss of accuracy compared to time domain calculations.

This paper aims to address the technology gap by developing a practical and accurate method for fatigue assessment of offshore wind turbines. Based on this idea, fatigue damage of Jacket support structures of OWT under combined wind loading and wave loading is studied. A half coupling methodology is proposed to carry out the dynamic response by considering aerodynamic and structural damping. Implementation of decoupling model is conducted based on FAST and ANSYS. Combined stress response spectra are obtained. Finally, fatigue damage is calculated with general spectral methods and the method previously proposed by the authors.

2 Basic Description of fatigue analysis

2.1 Spectral parameter of random process

In this paper, wind and wave are assumed as Gaussian random processes with zero mean. The basic characterization of random process can be denoted with spectral moments. The most commonly used spectral parameters are the *0*-th-order, *1*-th-order, *2*-th-order, *4*-th-order, e.g., λ_0, λ_1, λ_2, λ_4, which is defined as Eq. (1)

$$\begin{aligned} \lambda_0 &= \int_0^\infty S_X(\omega)d\omega, \qquad \lambda_1 = \int_0^\infty \omega \cdot S_X(\omega)d\omega \\ \lambda_2 &= \int_0^\infty \omega^2 \cdot S_X(\omega)d\omega, \quad \lambda_4 = \int_0^\infty \omega^4 \cdot S_X(\omega)d\omega \end{aligned} \tag{1}$$

where $S_X(\omega)$ is the power spectral density function.

Two bandwidth parameters which describe a random process are given as

$$\alpha_1 = \frac{\lambda_1}{\sqrt{\lambda_0\lambda_2}}, \quad \alpha_2 = \frac{\lambda_2}{\sqrt{\lambda_0\lambda_4}} \tag{2}$$

where α_1 is the Vanmarcker's bandwidth parameter, and α_2 is the irregularity factor.

Two spectral parameters, relating to α_1 and α_2, are defined as follows [25-27]:

$$\delta = \sqrt{1-\alpha_1^2} = \sqrt{1-\frac{\lambda_1^2}{\lambda_0\lambda_2}}, \quad \varepsilon = \sqrt{1-\alpha_2^2} = \sqrt{1-\frac{\lambda_2^2}{\lambda_0\lambda_4}} \tag{3}$$

where δ is Vanmarcke's spectral parameter with $0 \le \delta \le 1$, and ε is Wirsching's spectral width parameter with $0 \le \varepsilon \le 1$.

Other typical parameters are the mean zero up-crossing frequency ν_0 and the peak occurrences frequency ν_p, which depend on spectral moments in frequency domain and can be determined:

$$\nu_0 = \frac{1}{2\pi}\sqrt{\frac{\lambda_2}{\lambda_0}},\ \nu_p = \frac{1}{2\pi}\sqrt{\frac{\lambda_4}{\lambda_2}} \tag{4}$$

2.3 Spectral fatigue analysis theory of random process

Fatigue analysis method widely used in ship and ocean engineering is the *S–N* curve method which is given as [28-29]:

$$N = K \cdot S^{-m} \tag{5}$$

where *K* represents the fatigue strength coefficient, and *m* are the fatigue strength exponent.

Fatigue damage is commonly calculated with a linear accumulation hypothesis by Palmgren and Miner [30] as:

$$D = \sum \frac{n_i}{N_i} = \frac{1}{K}\sum n_i S_i^m \tag{6}$$

where n_i is the number of cycles in the *i-th* stress level S_i, obtained with a rainflow counting method for a random stress process [31]; N_i is the number of cycles at fatigue failure for the stress S_i.

For a continuum stress amplitude with a probability density function (PDF) $f_S(S)$, fatigue damage during the time T can be calculated as Eq. (7)

$$D = \frac{\nu_c \cdot T}{K} \int_0^\infty S^m \cdot f_S(S) dS \tag{7}$$

When $f_S(S)$ is an ideal narrow-band process, fatigue damage in Eq. (7) can be given with an analytical expression based on Rayleigh distribution assumption [32-33] as:

$$D_{NB} = \frac{\nu_0 \cdot T}{K} \left(\sqrt{2\lambda_0}\right)^m \Gamma\left(\frac{m}{2}+1\right) \tag{8}$$

Where $\Gamma(\cdot)$ is the Gamma function.

When $f_S(S)$ is a wide-band process, fatigue damage can be calculated by a bandwidth correction [27].

$$D_{WB} = \rho \cdot D_{NB} \tag{9}$$

3 Development of half coupled model for fatigue assessment of OWTs

3.1 Fully coupling of equations of motion of wind turbine and support structure

For simplicity, the model of offshore wind turbine only considers aerodynamic and hydrodynamic loads which can be assessed as two independent, random vectorial inputs.

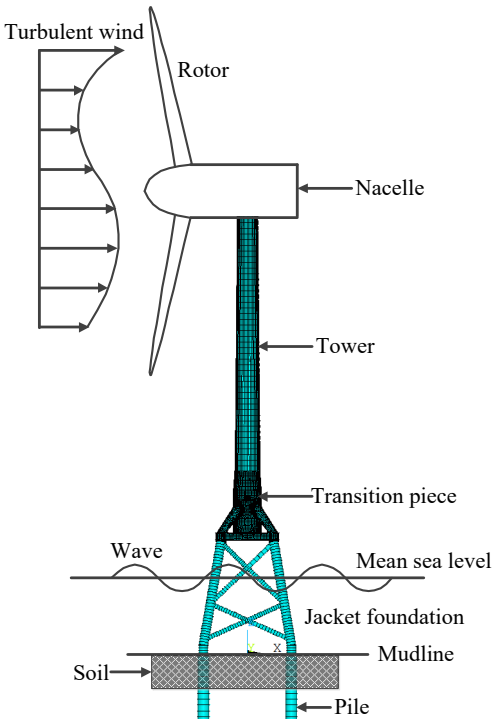

Fig. 1. Schematic diagram of Jacket offshore wind turbine

Modelling of the offshore wind turbine system comprises two distinct components: the wind turbine, the support structure with pile foundations. The fully coupling equations of motion modelled in FEM can be written as follows [18-19]:

$$\begin{aligned}&\left(\mathbf{M}_{WT}+\mathbf{M}_{SS}\right)\ddot{\boldsymbol{u}}(t)+\left(\mathbf{D}_{Stru}+\mathbf{D}_{Aero}+\mathbf{D}_{Hydro}+\mathbf{D}_{Soil}\right)\dot{\boldsymbol{u}}(t)+\left(\mathbf{K}_{WT}+\mathbf{K}_{SS}\right)\boldsymbol{u}(t)\\&=\mathbf{F}_{Aero}(t)+\mathbf{F}_{Hydro}(t)\end{aligned}\quad (10)$$

Where $\mathbf{M}$, $\mathbf{K}$ and $\mathbf{D}$ are, respectively, the mass, stiffness and damping matrices. $\ddot{\boldsymbol{u}}(t)$, $\dot{\boldsymbol{u}}(t)$ and $\boldsymbol{u}(t)$ are the acceleration, velocity and displacement vectors respectively. The system matrices and vectors are partitioned into blocks corresponding to the wind turbine (denoted by subscript *WT*) and support structure (subscript *SS*). $\mathbf{D}_{Stru}$ and $\mathbf{D}_{Aero}$ represent structural damping and aerodynamic damping respectively. $\boldsymbol{u}(t)$ is

represented by $\boldsymbol{u}=\begin{bmatrix}\boldsymbol{u}^{WT}\\ \boldsymbol{u}^{SS}\end{bmatrix}$, where $\boldsymbol{u}^{WT}$ represents the six rigid-body displacements of the wind turbine, and $\boldsymbol{u}^{SS}$ is the displacements of the support structure. $\mathbf{F}_{Aero}(t)$ is the aerodynamic force vector due to turbulent wind, and $\mathbf{F}_{Hydro}(t)$ is the hydrodynamic force vector due to wave.

3.2 Half coupling model

Fully coupling analysis of offshore wind turbine need to consider the coupling effects between environmental loads, operating conditions and structural response. Hence, the random aerodynamic and hydrodynamic loadings are assumed to be independent. Considering the constitution of coupling equations of motion in Eq. (10), Aerodynamic damping, structural damping, soil damping, hydrodynamic damping, stiffness terms and a hydrodynamic inertia term are contained in the system matrices. Therefore, the decoupling process will depend on the above conditions which will be described in the following section in detail.

(1) Aerodynamic damping

Aerodynamic damping is induced by the operating rotor. It is related to the interaction between the support structure and the wind turbine. Decoupling of wind response and wave response depends on the aerodynamic damping. Hence, in decoupled model, aerodynamic damping will be an important factor affecting the rationality of fatigue damage of OWT structure.

(2) Structural damping

Structural damping is also named as modal damping and the common sources include internal material friction and bolted or welded joints. It should also be considered in the half decoupled model. Typical value with a 1% of damping is selected for OWT structure [6].

(3) Hydrodynamic loading

Hydrodynamic damping is caused by the rigid structural motion and mainly due to the viscous drag force on flexible, submerged members as cables and risers. Jacket support structure studied in this paper is relatively stiff below the water surface. Therefore, the effect of hydrodynamic damping can be approximately equal to zero.

(4) Soil damping

A simplified model with apparent fixity length is adopted to consider the effect of soil damping which is schematically illustrated in Fig. 2. For general calculations of soil condition, the fixity length is equal to 6D, in which D is the outer pile diameter [32-33].

Based on the discussion, the decoupling process firstly starts with the linearization of aerodynamic loads from rotor into concentrated forces. The aerodynamic loads can be calculated with a combination of blade element and momentum (BEM) theory. In Bladed, the aeroelastic model was established and aerodynamic calculation was carried out to obtain the load. After that, Rotor-Nacelle Assembly (RNA) will be

assumed to be rigid body and be represented with a lumped mass at the top of the tower. The static component of the condensed aerodynamic forces can be directly applied at the tower top as an external force independent of the tower top velocities as shown in Fig.2. As a result, the equations of motion for the decoupled model with rigid blades can be written as

$$\begin{aligned}&\left(\mathbf{M}_{WT}+\mathbf{M}_{SS}\right)\ddot{\boldsymbol{u}}\left(t\right)+\left(\mathbf{D}_{Stru}+\mathbf{D}_{Aero}\right)\dot{\boldsymbol{u}}\left(t\right)+\left(\mathbf{K}_{WT}+\mathbf{K}_{SS}\right)\boldsymbol{u}\left(t\right)\\&=\mathbf{F}_{Aero}^{Rigid}\left(t\right)+\mathbf{F}_{Hydro}\left(t\right)\end{aligned}\tag{11}$$

In which $\mathbf{F}_{Aero}\left(t\right)=\mathbf{F}_{Aero}^{Rigid}\left(t\right)=\left[F_x\left(t\right)\ F_y\left(t\right)\ F_z\left(t\right)\ M_x\left(t\right)\ M_y\left(t\right)\ M_z\left(t\right)\right]$

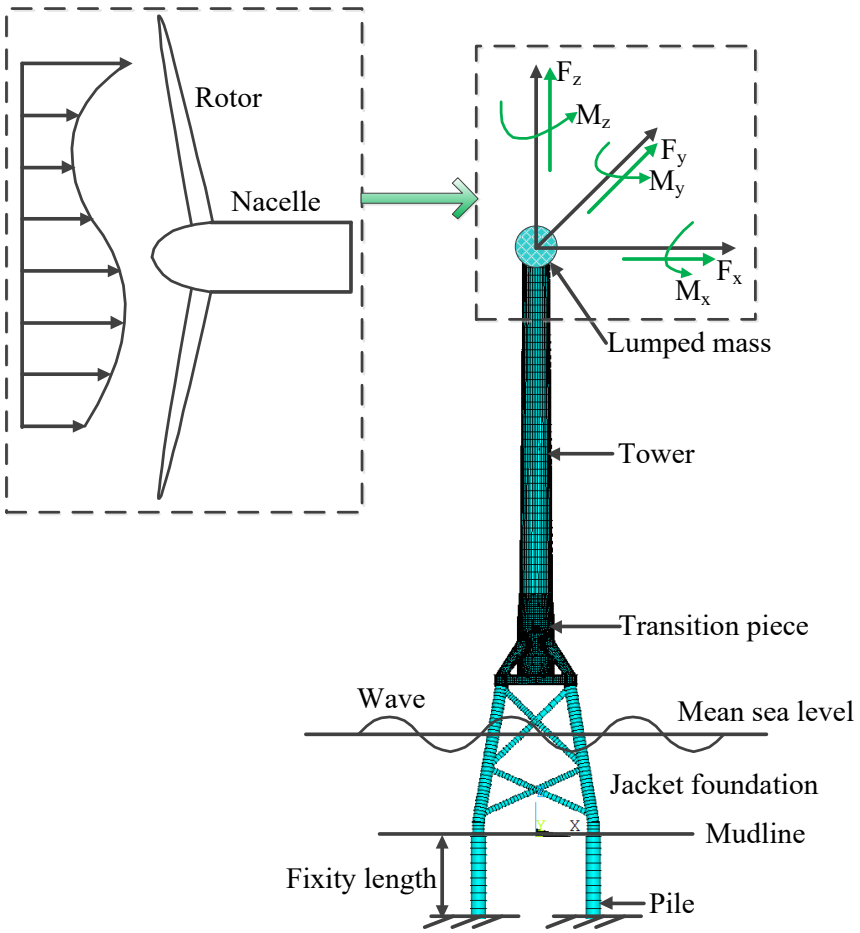

Fig. 2. The decoupling of the aerodynamic forces at tower top

3.3 Implementation of half coupling model

The above description about half coupling model is a theoretical process, and then it is necessary to combine the means of finite element analysis and utilizing commercial general software to execute the entire process of the half coupling analysis.

Based on the fully coupling and decoupling equation, several integrated and semi-integrated design tools are developed as shown in Table 1.

(1) Bladed+SACS

Support structure was built in Structural analysis computer system (SACS), imported to Bladed. Wind wave current and soil stiffness are imported into Bladed and wind turbine structure model is built. The aerodynamic load and wave load are calculated in Bladed and imported into SACS to carry out fatigue analysis. This treatment is not suitable for bearing platform and requires extensive work for load transfer.

(2) FAST+SACS

FAST is used as the load solver in the overall analysis process, and the load is imported to ANSYS for dynamic response calculation of Jacket support structure. Since FAST is open source, a half- and fully coupling analysis of FAST+ANSYS can be realized by compiling the calling interface. This treatment is required to establish a working environment of FAST.

Table 1 Different design tools

Design tool	Method	Application

Bladed+SACS	Half coupling	Jacket foundation
FAST+SACS	Fully coupling	Jacket foundation
FAST+ANSYS	Half coupling	Jacket foundation and bearing platform
Bladed+ANSYS (Present)	Half coupling	Jacket foundation and bearing platform

(3) The present tool: Bladed+ANSYS

Two main softwares including Bladed and ANSYS are used in this paper. The specific implementation steps are described in Fig. 3.

Firstly, an environmental condition should be established. For a simplified analysis, wind and wave will be assumed as collinear and omnidirectional. Thus, the environmental condition can be represented with a three-dimensional scatter diagram which describes a probability distribution of a significant wave height, zero-crossing period and mean wind speed.

Next, selecting an environmental case and giving a mean wind speed V, the relevant wind load information can be obtained through the Bladed calculation, and then combining with harmonic response analysis in ANSYS, the stress response under the turbulent wind load can be calculated. Similarly, giving a significant wave height H and zero-crossing period T under the same case, the stress response spectrum under wave load can be obtained through linear spectral analysis in SACS.

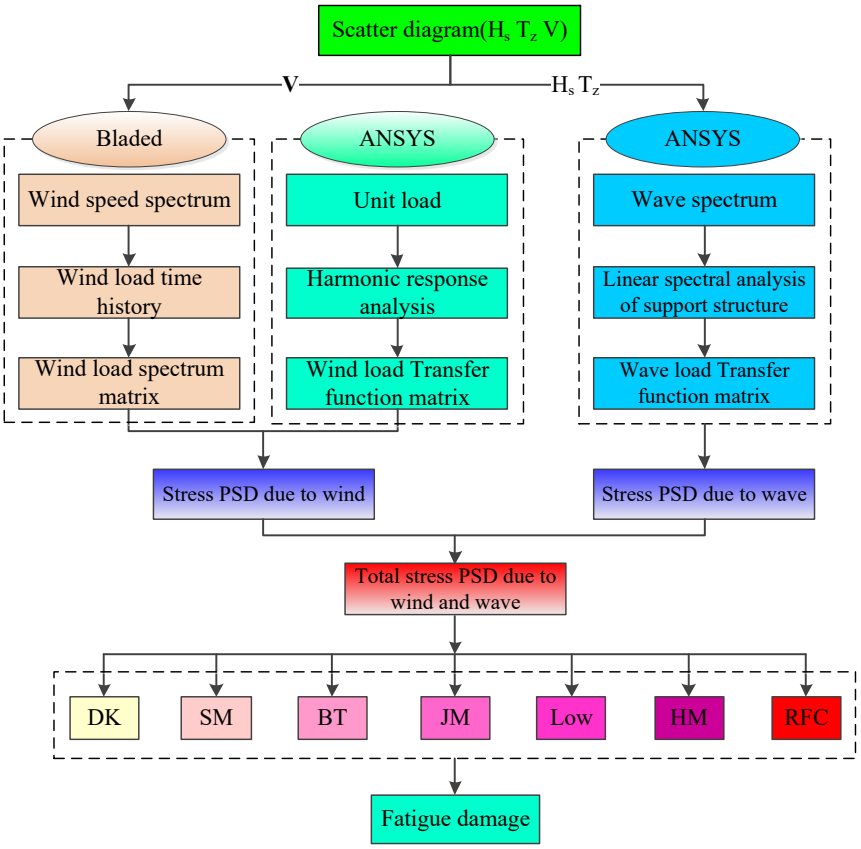

Fig. 3. Flowchart of half coupling analysis method for fatigue damage assessment

The total response spectra due to wind loading and due to wave loading are calculated independently, and then the combined response spectrum can be obtained by simple summation of the corresponding spectra. Using this spectrum, several spectral methods can be used to derive the fatigue damage as shown in Fig. 3. Rainflow counting is considered as an accurate solution and is incorporated in this paper for reference.

4 Frequency domain solution of half coupled model for jacket offshore wind turbine

4.1 Modelling of support structure of OWT

As shown in Fig. 1, the wind turbine support structure consists of the tower, the

transition piece, and the jacket-type foundation. The main parameters can be seen in Table 2. The finite element model of offshore wind turbine is built in ANSYS. The element type is Beam188, shell63, pipe59 and pipe16, corresponding to the tower, the transition piece, the jacket-type foundation and the pile, respectively. The finite element model includes 36123 nodes and 34736 elements. The element size is set according to DNV-RP-C203 [29]. A refine mesh of t * t (t is the plate thickness) is made at the hot spot region of welded tubular joints. A relatively coarse mesh is used at other region. The detailed model is shown in Fig. 4. The rotor and blade on the top of the tower are represented with a lumped mass. Soil-pile behaviour is addressed as linear through fixing the bottom of pile at the length of six times pile diameter. In addition, the aerodynamic damping and the critical damping is set to 4% and 1% respectively [6, 18].

Table 2 Principal characteristics of structural members [34]

	Length (m)	Diameter (m)	Thickness (m)
Tower	75		
Transition structure	10	4.2	0.05
Chord	25	1.79	0.03
Brace	25	0.61	0.01
Transition structure	10	4.2	0.05
Pile	10.74	1.79	0.03

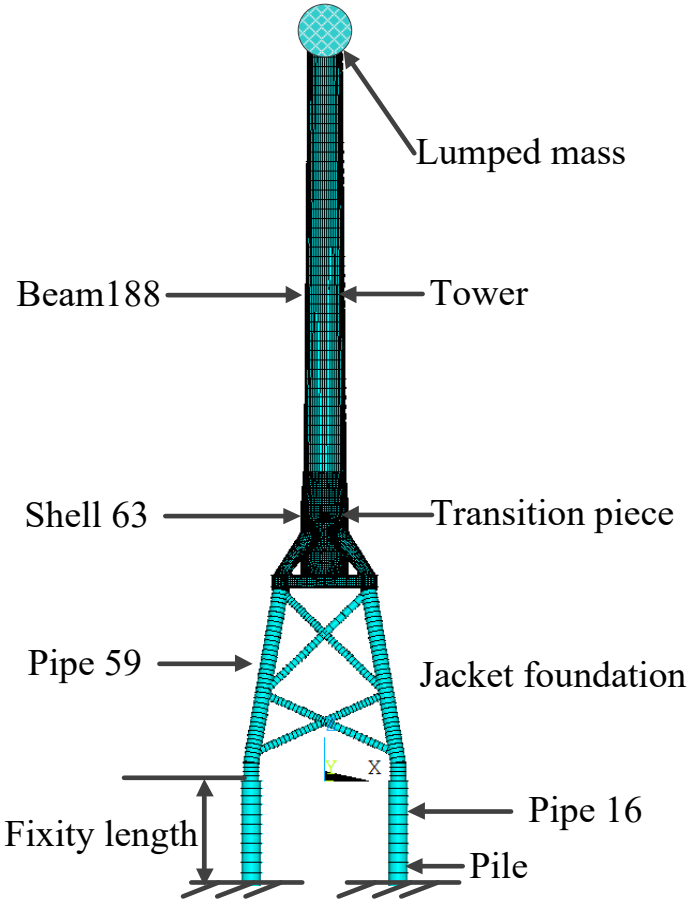

Fig. 4. The finite element model of offshore wind turbine

4.2 Frequency domain analysis based on half coupled model under wind loading

4.2.1 Frequency domain analysis of offshore wind turbine under wind loading

In order to obtain the stress response spectrum for fatigue damage estimation under wind loading, a dynamic analysis of the jacket support structure of OWT is carried out. The detailed process can be seen in Fig.5.

The first step is to select a suitable wind spectrum. The von Kármán spectrum is used as the wind speed spectrum in this paper [35]. The von Kármán model is based on the mean wind speed, the turbulence intensity, and a length scale:

$$S_{Karman}(f)=\frac{\sigma_v^2 4L_v/V_w}{\left(1+70.8\left(fL_v/V_w\right)^2\right)^{5/6}} \tag{12}$$

The detailed parameter setting can be found in the literature [34].

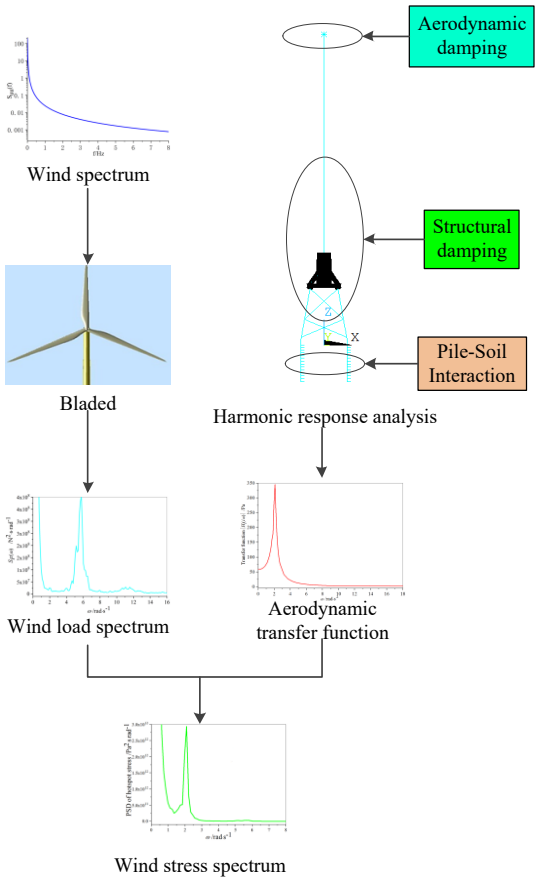

Fig. 5. Flowchart of the frequency domain calculation to determine the stress spectrum due to wind loading

According to the defined parameters, the self-spectral density formula can be seen in Fig. 6.

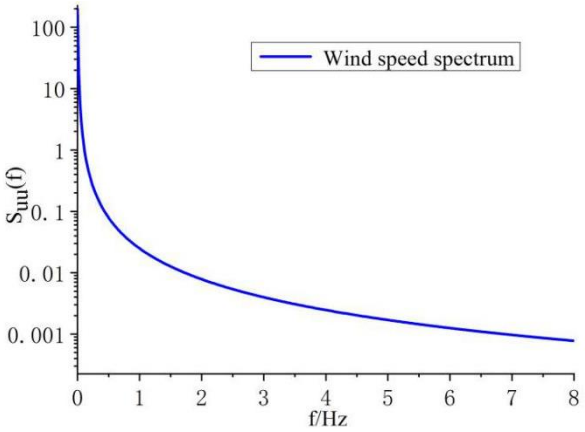

Fig. 6. Wind spectrum by von Kármán

According to the given wind speed spectrum, the wind load spectrum can then be

obtained via Fourier transform in Bladed. Taking loads F_x as an example, the corresponding auto PSD is shown in Fig. 7.

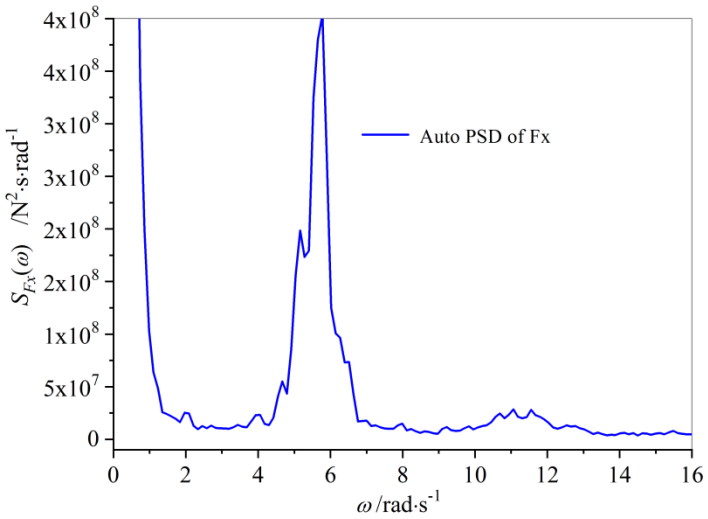

Fig. 7. Auto PSD of wind load component Fx

The following step is to obtain the transfer function of the hotspot stress which will be calculated according to the method in the literature [34]. The ANSYS software can be used to calculate stress amplitude of the hotspot location due to a unit load with a harmonic response analysis. When the load spectrum at the tower top is given, the transfer function can be derived by dividing the load spectrum and taking the square root:

$$TRF = \sqrt{\frac{S_\sigma(\omega)}{S_F(\omega)}} \tag{13}$$

Fig. 8 gives the transfer function of the hotspot stress under the load component F_x.

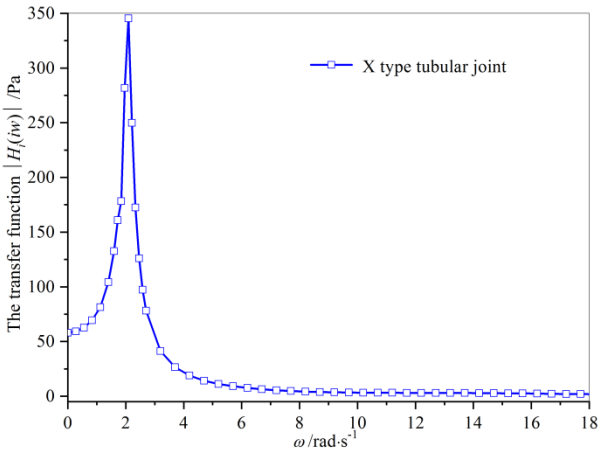

Fig. 8. Transfer function between wind load spectrum and tower top load

By multiplying the square of the transfer function with the input wind load spectrum, the hotspot stress response spectrum under six load components for an X-joint and a K-joint can be determined as shown in Figure 9. This calculation process is briefly summarized here. It was described in more detail in Reference [34].

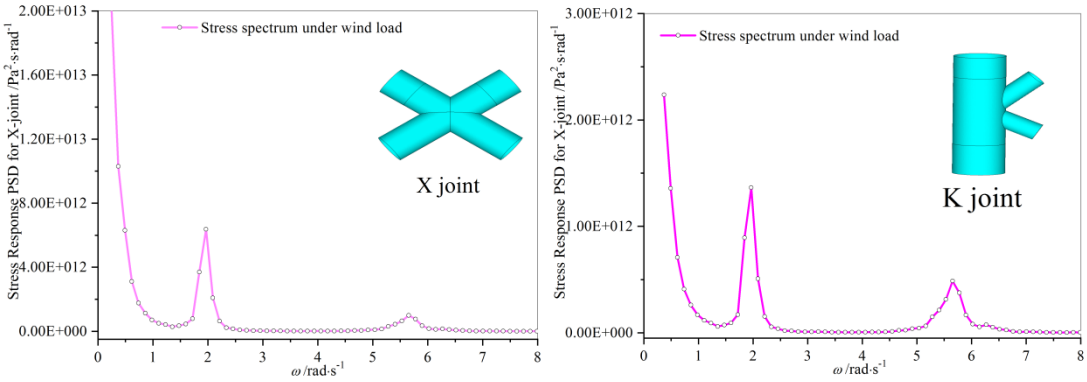

(a) X-type tubular joint (b) K-type tubular joint

Fig. 9. Stress response spectrum of (a) K-joint and (b) X-joint under wind loading

4.2.2 Validity verification of half coupled model

In order to verify the validity of the half coupled model, a time domain simulation with a fully coupled model will be carried out. In the fully coupled model, the pile-soil interaction is simulated by nonlinear springs, and the soil data (P-y curve, T-z curve, and Q-z curve) are obtained from actual engineering surveys. The fully coupled

time domain analysis is carried out by ANSYS software. The simulation parameter setting is as:

- 0.05 s time step for the analysis
- 600 seconds simulation time per wind speed

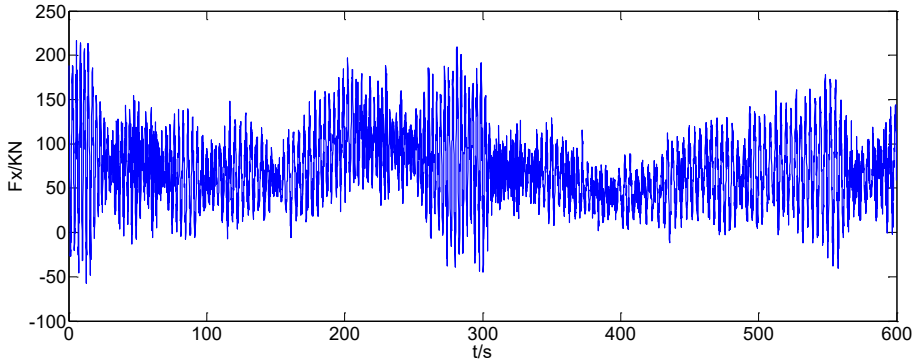

Fig. 10 600 seconds wind load history

By inputting the load time history as shown in Fig.10, the stress response can be obtained with a transient dynamic analysis. Then, the resulting stress time series can be transformed to a power spectral density function through a fast fourier transform. Fig. 11 compares the stress response for X tubular joint and K tubular joint obtained from the fully coupled model and half coupled model. It can be seen that the results for both methods match very well.

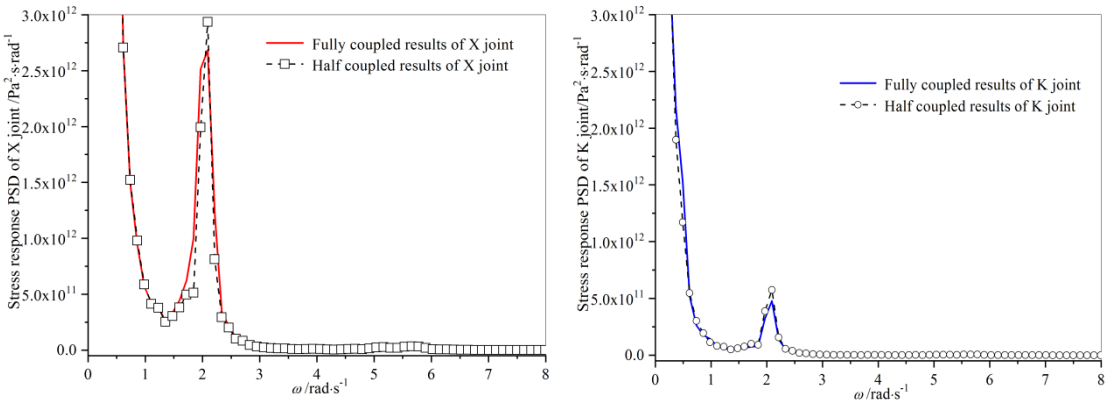

Fig. 11 Comparison of stress spectrum from HCM and FCM for X joint and K joint

A detailed comparison including some common spectral parameters between

HCM spectrum and FCM spectrum is listed in Table 2. Small differences can be found in Table, which demonstrate the validity of HCM.

Table 2 Comparison of spectral parameters from HCM and FCM

	Method	λ_0	λ_1	λ_2	λ_4	ε	ν_0	ν_p
X-joint	FCM	4.997	4.352	6.984	51.167	0.900	0.188	0.431
	HCM	4.888	4.026	6.298	48.387	0.912	0.181	0.441
K-joint	FCM	0.992	0.745	1.072	7.693	0.922	0.166	0.426
	HCM	0.955	0.784	1.212	8.983	0.910	0.179	0.433

More importantly, as shown in Table 3, under the same computer configuration, the computation duration time of HCM model is far shorter than that of FCM, which indicates that HCM performs better than FCM in terms of calculation speed. In addition, the space occupied by the generated files for HCM is far less than that for FCM, which is another advantage of HCM.

Table 3 Comparison of spectral parameters from HCM and FCM

	Processor	RAM Memory	Computation duration	Resulting file Storage space
FCM	Intel Core 7 3.7 GHz	16GB	48 hours	2 TB
HCM	Intel Core 7 3.7 GHz	16GB	0.1 hour	200MB

4.3 Frequency domain analysis based on half coupled model under wave loading

Frequency domain approach is the common practice for assessment of the fatigue of offshore wind turbine under wave loading, which includes the wave spectrum, linear spectral analysis and determination of stress response spectrum. The wave spectrum describes the random characteristics of waves and by multiplying that by the

square of the transfer function, the stress response spectrum is determined. The flowchart of frequency domain analysis can be seen in Fig.12. Frequency domain analysis requires the structure system is linear, however, the wave load based on Morison equation is non-linear. Therefore, the linearization of Morison equation will be developed and be the focus of this part.

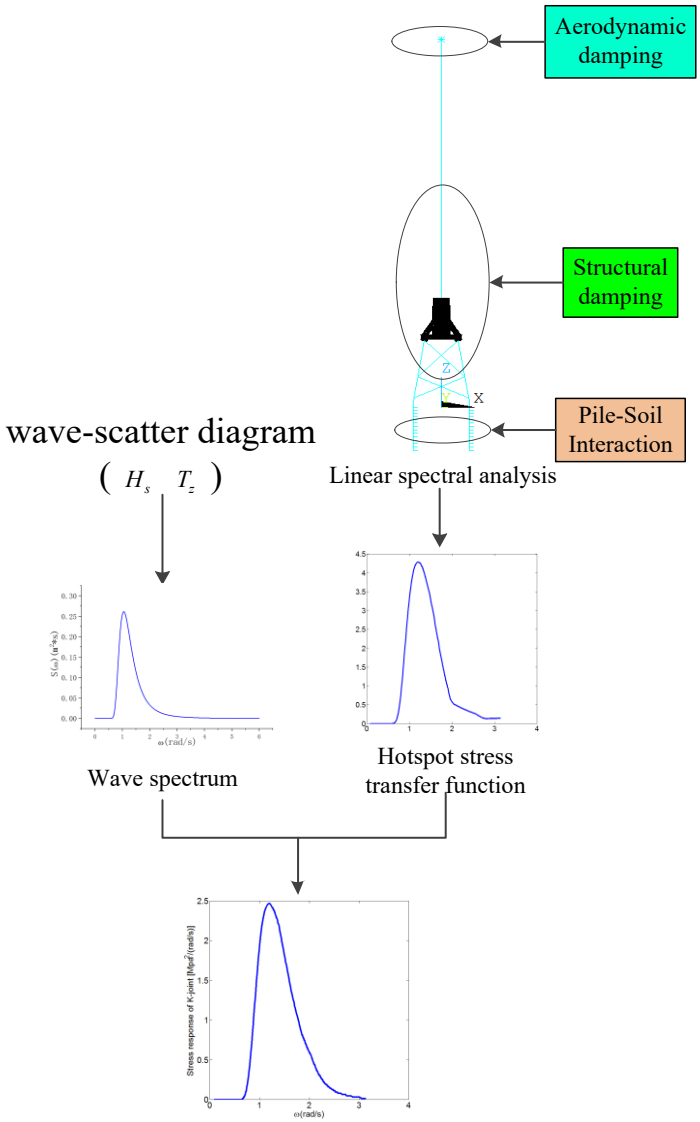

Fig. 12. Flowchart of the frequency domain calculation to determine the stress spectrum due to wave loading

When calculating wave loads, a non-linear term by the drag force is introduced in

Morison equation which will effect the calculation results of wave loads in the frequency domain. However, ANSYS software does not linearize Morison equation. Therefore, it is very critical to finish the linearization of non-linear wave loads in ANSYS.

According to Airy wave theory, non-linear Morison wave loads will be linearized as:

$$f(t) = f_D(t) + f_I(t) = \frac{1}{2}\rho_w C_D D\sigma_u \sqrt{\frac{8}{\pi}}u(t) + C_M \rho_w \frac{\pi}{4} D^2 a(t) \tag{14}$$

$f_D(t)$ is drag force; $f_I(t)$ is inertial force; C_D is drag coefficient; C_M is inertial coefficient; $u(t)$ is water particle velocity; $a(t)$ is water particle acceleration; ρ_w is water density; D is diameter of a single cylinder.

$u(t)$ and $a(t)$ can be denoted as follow:

$$u(t) = \left[\omega \frac{\mathrm{ch}\, k(z+d)}{\mathrm{sh}kd}\right]\eta(t) \tag{15}$$

$$a(t) = \left[\omega^2 \frac{\mathrm{ch}\, k(z+d)}{\mathrm{sh}kd}\right]\eta(t+\frac{T}{4}) \tag{16}$$

From the above equation, the transfer function of water particle velocities and accelerations

$$T_u(\omega) = \omega \frac{\mathrm{ch}\, k(z+d)}{\mathrm{sh}kd} \tag{17}$$

$$T_a(\omega) = \omega^2 \frac{\mathrm{ch}\, k(z+d)}{\mathrm{sh}kd} \tag{18}$$

Velocity spectral density and acceleration spectral density at height z can be

given in:

$$S_u(\omega) = \left|T_u(\omega)\right|^2 S_\eta(\omega) \tag{19}$$

$$S_a(\omega) = \left|T_a(\omega)\right|^2 S_\eta(\omega) \tag{20}$$

The relationship between the auto-correlation function of the drag force and the auto-correlation function of water particle velocities $u(t)$ is defined as:

$$f_D(t) \cdot f_D(t+\tau) = \left(\frac{1}{2}\rho_w C_D D \sigma_u \sqrt{\frac{8}{\pi}}\right)^2 u(t) \cdot u(t+\tau) \tag{21}$$

The relationship between the auto-correlation function of the inertial force and the auto-correlation function of water particle accelerations $a(t)$ is defined as:

$$f_I(t) \cdot f_I(t+\tau) = \left(C_M \rho_w \frac{\pi}{4} D^2\right)^2 a(t) \cdot a(t+\tau) \tag{22}$$

Hence the drag force spectrum $S_{fD}(\omega)$ can be obtained through a Fourier transform as:

$$S_{fD}(\omega) = \left(\frac{1}{2}\rho_w C_D D \sigma_u \sqrt{\frac{8}{\pi}}\right)^2 S_u(\omega) \tag{23}$$

The inertial force spectrum $S_{fI}(\omega)$ can be obtained through a Fourier transform as:

$$S_{fI}(\omega) = \left(C_M \rho_w \frac{\pi}{4} D^2\right)^2 S_a(\omega) \tag{24}$$

Substituting Eqs. (19-20) into Eqs. (23-24), the drag force spectrum and inertial force spectrum can be further expressed as:

$$S_{fD}(\omega)=\left(\frac{1}{2}\rho_w C_D D\sigma_u\sqrt{\frac{8}{\pi}}\right)^2\left(\omega\frac{\mathrm{ch}\,k(z+d)}{\mathrm{sh}kd}\right)^2 S_\eta(\omega) \tag{25}$$

$$S_{fI}(\omega)=\left(C_M\rho_w\frac{\pi}{4}D^2\right)^2\left(\omega^2\frac{\mathrm{ch}\,k(z+d)}{\mathrm{sh}kd}\right)^2 S_\eta(\omega) \tag{26}$$

The transfer function of velocity spectral density and acceleration spectral density can be derived as:

$$T_{fD}(\omega)=\frac{1}{2}\rho_w C_D D\sigma_u\sqrt{\frac{8}{\pi}}\omega\frac{\mathrm{ch}\,k(z+d)}{\mathrm{sh}kd} \tag{27}$$

$$T_{fI}(\omega)=C_M\rho_w\frac{\pi}{4}D^2\omega^2\frac{\mathrm{ch}\,k(z+d)}{\mathrm{sh}kd} \tag{28}$$

Wave force spectrum on a single cylinder per unit length can be derived as:

$$\begin{aligned}S_f(\omega)=&\left(\frac{1}{2}\rho_w C_D D\sigma_u\sqrt{\frac{8}{\pi}}\omega\frac{\mathrm{ch}\,k(z+d)}{\mathrm{sh}kd}\right)^2 S_\eta(\omega)\\&+\left(C_M\rho_w\frac{\pi}{4}D^2\omega^2\frac{\mathrm{ch}\,k(z+d)}{\mathrm{sh}kd}\right)^2 S_\eta(\omega)\end{aligned} \tag{29}$$

Irregular waves can be regarded as the superposition of regular waves of different amplitudes and frequencies. So that when the wave lift is as a stationary random process, the linearized Morrison force will also be a stationary random process. Therefore, wave load on a single cylinder in a unit length can be calculated with integration on the cylinder, and then the transfer function of wave force is obtained as:

$$T_F(\omega)=\left\{\begin{aligned}&\left(\frac{1}{2}\rho_w C_D D\sqrt{\frac{8}{\pi}}\frac{\omega}{\mathrm{sh}kd}\int_{z1}^{z2}\sigma_u(z)\,\mathrm{ch}\,k(z+d)dz\right)^2\\&+\left(C_M\rho_w\frac{\pi}{4}D^2\frac{\omega^2}{\mathrm{sh}kd}\int_{z1}^{z2}\mathrm{ch}\,k(z+d)dz\right)^2\end{aligned}\right\}^{1/2} \tag{30}$$

According to linear spectral analysis, stress response spectrum under wave loading can be obtained. In this paper, stress spectra of two typical tubular joints (K-joint and X-joint) are calculated as shown in Fig. 13.

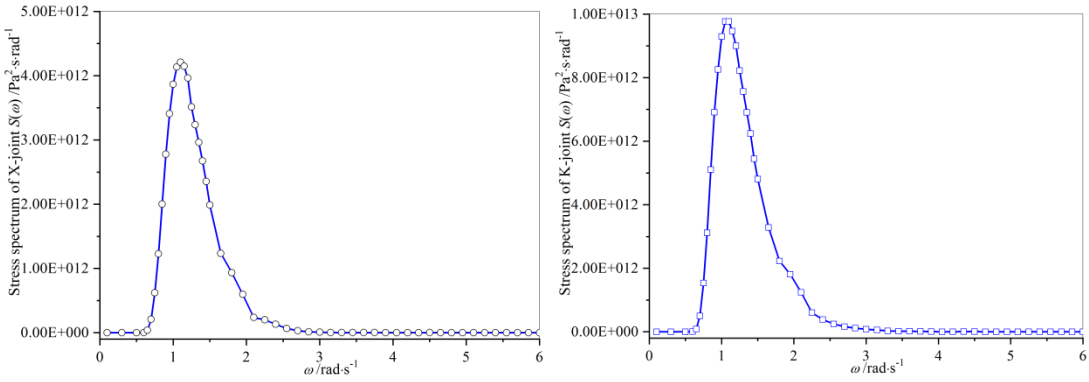

(a) X-type tubular joint (b) K-type tubular joint

Fig. 13. Stress response spectrum of (a) K-joint and (b) X-joint under wave loading

5 Fatigue Damage assessment

After obtaining the wind and wave stress response, the combined stress spectrum can be added linearly. Then, a new problem arises that how to calculate fatigue life using the power spectral density (PSD) of stresses. However, stress response due to wind loading is commonly a broad banded process while the stress response due to wave loading is also a wide process, so that a narrowband assumption method will produce too conservative fatigue damage results. In that situation, it is challenging for designers to evaluate fatigue damage under combination of wind and wave loading. Fortunately, many researchers including the author proposed some methods to correct and improve narrowband fatigue damages. However, these methods have different accuracy, scope of application and complexity. This section aims at looking for a

simple, practical and precise fatigue damage assessment technique which can account for the interaction between wind and wave response. Six typical and representative methods: Dirlik, Single-moment, Benasciutti-Tovo method, Jiao-Moan method, Lows bimodal method, Han-Ma method proposed by the author [36-41] will be applied to calculate fatigue damage of OWT as seen in table 4. Their solutions will be compared with rainflow counting fatigue damage solution.

Table 4 different fatigue damage models

Fatigue damage model	Expression
Dirlik (DK) method [36]	$p_{Dirlik}(S)=\frac{1}{(\lambda_0)^{\frac{1}{2}}}\left[\frac{G_1}{Q}\exp\left(-\frac{z}{Q}\right)+\frac{G_2 z}{\gamma^2}\exp\left(-\frac{z^2}{2\gamma^2}\right)+G_3 z\exp\left(-\frac{z^2}{2}\right)\right]$
Single-moment (SM) method[37]	$D_{SM}=\frac{2^{\frac{m}{2}}T}{2\pi K}\Gamma\left(\frac{m}{2}+1\right)(\lambda_{2/m})^{\frac{m}{2}}$
Benasciutti and Tovo (BT) method[38]	$D_{RFC}=\left[b+(1-b)\alpha_2^{m-1}\right]D_{NB}=\rho_{BT}D_{NB}$
Jiao-Moan (JM) method[39]	$\rho_{JM}=\frac{\nu_{0,P}}{\nu_0}\times\left[\lambda_{0,L}^{*\frac{m}{2}+2}(1-\sqrt{\frac{\lambda_{0,\mathrm{H}}^*}{\lambda_{0,L}^*}})+\sqrt{\pi\lambda_{0,L}^*\lambda_{0,\mathrm{H}}^*}\frac{m\Gamma(\frac{m}{2}+\frac{1}{2})}{\Gamma(\frac{m}{2}+1)}\right]+\frac{\nu_{0,\mathrm{H}}}{\nu_0}\lambda_{0,H}^{*\frac{m}{2}}$
Low's bimodal (LB) method[40]	$D_{LB}=D_s+D_l$
The present spectral combination rule[41]	$D_{HM}=\left(D_{wind}^{2/m}+D_{wave}^{2/m}\right)^{m/2}$

5.1. Dirlik (DK) method

Dirlik gives a PDF of rainflow amplitude after extensive numerical simulations [36]. This formula is a weight summation of an exponential distribution, a Rayleigh distribution and a standard Rayleigh distribution as:

$$p_{Dirlik}(S)=\frac{1}{(\lambda_0)^{\frac{1}{2}}}\left[\frac{G_1}{Q}\exp\left(-\frac{z}{Q}\right)+\frac{G_2 z}{\gamma^2}\exp\left(-\frac{z^2}{2\gamma^2}\right)+G_3 z\exp\left(-\frac{z^2}{2}\right)\right] \quad (31)$$

Where

$$z = \frac{S}{\sqrt{\lambda_0}} \tag{32}$$

is a standardized amplitude and:

$$x_m = \alpha_1 \cdot \alpha_2, \quad Q = \frac{1.25(\alpha_2 - \mathrm{G}_3 - \mathrm{G}_2\,\gamma)}{G_1}, \quad \gamma = \frac{\alpha_2 - x_m - G_1^2}{1 - \alpha_2 - G_1 + G_1^2} \tag{33}$$

$$G_1 = \frac{2\left(x_m - \alpha_2^2\right)}{1 + \alpha_2^2}, \quad G_2 = \frac{1 - \alpha_2 - G_1 + G_1^2}{1 - \gamma}, \quad G_3 = 1 - G_1 - G_2 \tag{34}$$

Fatigue damage based on Dirlik model can be given in a closed-form form as:

$$D_{Dirlik} = \frac{\nu_p T}{K}\left(\lambda_0\right)^{\frac{m}{2}}\left[D_1 Q^m \frac{1}{\sqrt{\pi}}\Gamma\left(\frac{m+1}{2}\right) + D_2 \gamma^m \Gamma\left(1 + \frac{m}{2}\right) + D_3 \Gamma\left(1 + \frac{m}{2}\right)\right] \tag{35}$$

5.2. Single-moment (SM) method

SM method is formulated on the basis of observation for extensive simulated data from rainflow analysis of bimodal PSD [37]. The formula is given as:

$$D_{SM} = \frac{2^{\frac{m}{2}} T}{2\pi K}\Gamma\left(\frac{m}{2} + 1\right)\left(\lambda_{2/m}\right)^{\frac{m}{2}} \tag{36}$$

The advantage of SM method is only one spectral moment $\lambda_{2/m}$ needs to be calculated.

5.3. Benasciutti and Tovo (BT) method

It is noted that the rainflow fatigue damage always has a lower and upper bound. Thus, BT gives a fatigue damage prediction model as [38]:

$$D_{RFC} = \left[b + (1-b)\alpha_2^{m-1}\right] D_{NB} = \rho_{BT} D_{NB} \tag{37}$$

Where the bandwidth correction factor can be obtained:

$$\rho_{BT} = b + (1-b)\alpha_2^{m-1} \tag{38}$$

in which an approximate formula of the weighted factor b is given in Eq. (39).

$$b = \frac{(\alpha_1 - \alpha_2)[1.112(1 + \alpha_1\alpha_2 - (\alpha_1 - \alpha_2))\exp(2.11\alpha_2) + (\alpha_1 - \alpha_2)]}{(\alpha_2 - 1)^2} \tag{39}$$

5.4. Jiao-Moan (JM) method

Jiao and Moan [39] derived a bandwidth correction factor from the envelope process of two narrow-banded Gaussian processes. The expression of this factor is given as:

$$\rho_{JM} = \frac{\nu_{0,P}}{\nu_0} \times \left[\lambda_{0,L}^{*\,\frac{m}{2}+2} (1 - \sqrt{\frac{\lambda_{0,\mathrm{H}}^*}{\lambda_{0,L}^*}}) + \sqrt{\pi \lambda_{0,L}^* \lambda_{0,\mathrm{H}}^*} \frac{m\Gamma(\frac{m}{2} + \frac{1}{2})}{\Gamma(\frac{m}{2} + 1)} \right] + \frac{\nu_{0,\mathrm{H}}}{\nu_0} \lambda_{0,H}^{*\,\frac{m}{2}} \tag{40}$$

Where $\lambda_{0,L}^*$ and $\lambda_{0,\mathrm{H}}^*$ are normalized zero-order spectral moments and $\nu_{0,P}$ is defined in Eq. (41)

$$\nu_{0,P} = \lambda_{0,L}^* \nu_{0,L} \sqrt{1 + \frac{\lambda_{0,\mathrm{H}}^*}{\lambda_{0,\mathrm{L}}^*} \left(\frac{\nu_{0,H}}{\nu_{0,\mathrm{L}}} \right)^2 \delta_H} \tag{41}$$

where

$$\delta_H = \sqrt{1 - \frac{\lambda_{1,\mathrm{H}}^{*\,2}}{\lambda_{0,H}^* \lambda_{2,H}^*}} \tag{42}$$

5.5. Low's bimodal (LB) method

Since two cycles can be extracted from rainflow counting, Low [40] proposed a

bimodal method as:

$$D_{LB} = D_s + D_l \tag{43}$$

Where D_s and D_l are related to the small and large cycles respectively.

Fatigue damage due to the small cycles is formulated as

$$\begin{aligned} D_s = {} & \frac{2^m \left(\nu_{0,H} - \nu_{0,L}\right) T}{K} \int_0^{\infty} \int_{\frac{\pi}{4\beta}}^{\frac{\pi}{2}} \int_{\varepsilon(r_L,\theta)}^{\infty} \left[r_H - \varepsilon\left(r_L,\theta\right)\right]^m \\ & \times f_{R_H}\left(r_H\right) f_{\Theta}\left(\theta\right) f_{R_L}\left(r_L\right) dr_H d\theta dr_L \end{aligned} \tag{44}$$

Where

$$\varepsilon\left(r_L,\theta\right) = \frac{\pi}{2\beta} r_L \sin\theta \tag{45}$$

$$f_{\Theta}\left(\theta\right) = \left(\frac{\pi}{2} - \frac{\pi}{4\beta}\right)^{-1}, \quad \frac{\pi}{4\beta} \le \theta \le \frac{\pi}{2} \tag{46}$$

The functions $f_{R_H}\left(r_H\right)$ and $f_{R_L}\left(r_L\right)$ are the Rayleigh distributions of the LF and HF components, respectively.

Fatigue damage due to the large cycles can be expressed as

$$\begin{aligned} D_l = {} & \frac{2^m \nu_{0,L} T}{K} \int_0^{\infty} \int_0^{\infty} \int_0^{\pi} \left[R_l\left(r_L, r_H, \psi\right)\right]^m \\ & \times f_{\psi}\left(\psi\right) f_{R_H}\left(r_H\right) f_{R_L}\left(r_L\right) d\psi dr_H dr_L \end{aligned} \tag{47}$$

Where

$$f_{\psi}\left(\psi\right) = \frac{1}{\pi}, \quad 0 \le \psi \le \pi \tag{48}$$

$$R_l = R_L \cos\left(\frac{\psi}{\beta}\right) + R_H \tag{49}$$

Eq. (44) and Eq. (47) must be calculated with numerical integral, and the innermost integral can be obtained according to Low's derivation.

5.6 The present spectral combination rule

Han and Ma [41] derived a simple and accurate formula for combination of fatigue damage subjected to two Gaussian random processes, based on this, a spectral combination rule is developed as:

$$D_{HM} = \left(D_{wind}^{2/m} + D_{wave}^{2/m} \right)^{m/2} \tag{50}$$

Where

$$D_{wind} = \frac{\nu_{0,wind} T}{K} \left(\sqrt{2\lambda_{0,wind}} \right)^m \Gamma\left(\frac{m}{2} + 1 \right) \tag{51}$$

$$D_{wave} = \frac{\nu_{0,wave} T}{K} \left(\sqrt{2\lambda_{0,wave}} \right)^m \Gamma\left(\frac{m}{2} + 1 \right) \tag{52}$$

Eq. (50) can also be expressed with a bandwidth correction factor as follow:

$$\rho_{HM} = \frac{\left(\nu_{0,wind}^{2/m} \cdot \lambda_{0,wind} + \nu_{0,wave}^{2/m} \cdot \lambda_{0,wave} \nu_{0,wave} \right)^{m/2}}{\nu_{0,X} \cdot \lambda_{0,X}^{m/2}} \tag{53}$$

Wind response and wave response can be taken as a low-frequency process and a high-frequency process respectively. The corresponding parameter in Eq. (53) can be calculated based on the stress response spectrum.

6 Results

In this paper, the bandwidth correction factor is used as a target to assess fatigue damage of support structures due to wind loads and wave loads. This factor can be defined as:

$$\rho = \frac{D_{com}}{D_{NB}} \tag{54}$$

D_{com} is the total fatigue damage obtained from JM method, LB method and HM method. D_{NB} is the fatigue damage based on narrowband approximation which can be given as,

$$D_{NB} = \nu_{0,wind+wave} \frac{T}{K} \left(\sqrt{2\lambda_{0,\mathrm{wind+wave}}} \right)^m \Gamma\left(\frac{m}{2} + 1 \right) \tag{55}$$

In which

$$\nu_{0,wind+wave} = \sqrt{\frac{\nu_{0,\mathrm{wind}}^2 \lambda_{0,\mathrm{wind}} + \nu_{0,\mathrm{wave}}^2 \lambda_{0,\mathrm{wave}}}{\lambda_{0,\mathrm{wind}} + \lambda_{0,\mathrm{wave}}}} \tag{56}$$

$$\lambda_{0,wind+wave} = \lambda_{0,wind} + \lambda_{0,wave} \tag{57}$$

According to the results of dynamic analysis, the mean zero up-crossing rate and the zeroth-order spectral moment of K-joints and X-joint corresponding to wind response in time domain and wave response in frequency domain can be extracted.

To compare the accuracy of the different methods, a percentage error of the damage value is introduced:

$$Error = \frac{\rho - \rho_{RFC}}{\rho_{RFC}} \cdot 100 \tag{58}$$

where ρ is the damage correction factor obtained by the spectral methods, and ρ_{RFC} is the corresponding numerical simulation result.

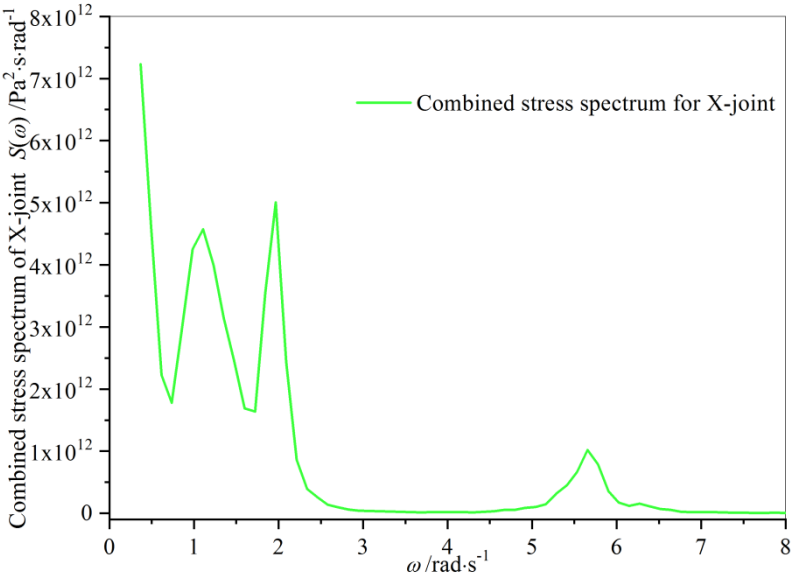

Fig.14. Combined stress spectrum of X-joint

Through the decoupling of the turbine and the support structure, wind and wave induced response can be determined separately. The effects of wind and wave response can then be added by simple summation of the corresponding spectra. Figure 14 is the stress spectrum of a typical X-joint in the jacket-type offshore wind turbine support structure, which is obtained through half coupling analysis theory and finite element method. This stress spectrum shows a characterization of multiple peaks which is induced by combined wind and wave loads. The bandwidth of wind spectrum and wave spectrum can be calculated respectively, corresponding to $\varepsilon_{\text{wave}}$=0.5182, $\varepsilon_{\text{wind}}$=0.9351. It can be seen that stress spectra by wind and wave are rather broadband processes.

Table 5 lists the relative error of different fatigue assessment methods according to Eq. (58). Only the present method, BT method and DK method provide accurate fatigue damage predictions, with the errors -1.41%, -0.68% and -1.51% for m=3, and increasing to -8.59%, -6.69% and -3.16% for m=5 respectively. For SM method, the damage may be under-estimated by as much as about -12.9% for m=3 and -21.8% for

m=5. JM method, LB method and Low-2014 method on the other hand always return positive errors (with a maximum overestimation of about 25% for m=3 and 35% for m=5 for JM method, which indicates they are conservative design.

Table 5 Error of fatigue damage by different methods for m=3 and m=5 for X-joint

		JM	LB	Low-2014	The present method	SM	BT	DK	RFC
m=3	ρ	0.872	0.772	0.780	0.686	0.606	0.691	0.685	0.695
	Error/%	25.41	11.07	12.18	-1.41	-12.9	-0.68	-1.51	0.00
m=5	ρ	0.958	0.843	0.824	0.650	0.556	0.664	0.689	0.711
	Error/%	34.73	18.59	15.85	-8.59	-21.8	-6.69	-3.16	0.00

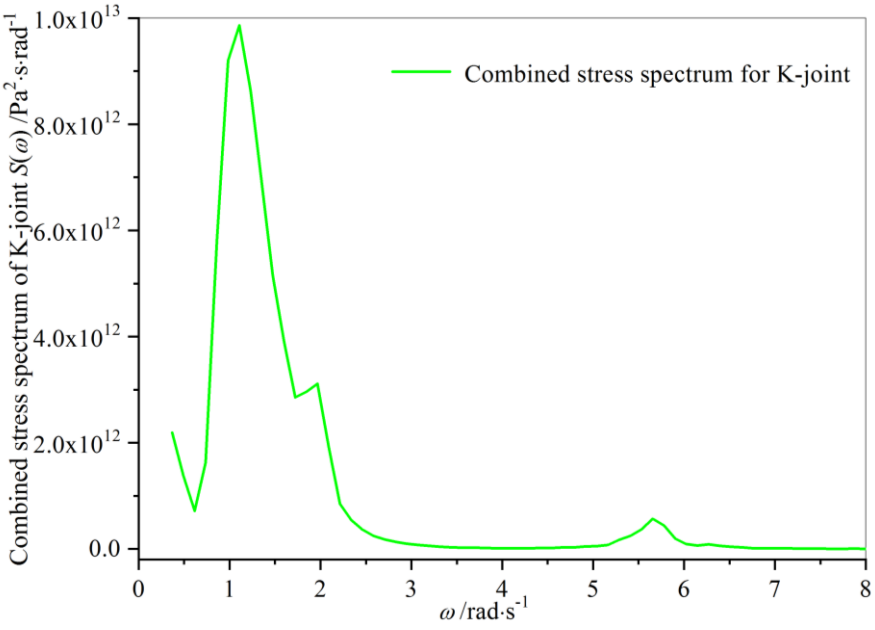

Fig. 15. Combined stress spectrum of K-joint

Figure 15 is the stress spectrum of a typical K-joint in the jacket-type offshore

wind turbine support structure. The bandwidth of wind spectrum and wave spectrum can be calculated respectively, corresponding to $\varepsilon_{\text{wave}}$=0.577, $\varepsilon_{\text{wind}}$=0.910. Table 5 shows the relative error of different fatigue assessment methods for K-joint.

A same tendency can be observed in Table 6. Only the present method, BT method and DK method give accurate fatigue damage predictions. For m=3, the errors are -3.35%, -1.58% and 0.03%; For m=5, the errors increases slight to -7.93%, -5.32% and -4.87% respectively. For SM method, the damage may be under-estimated by as much as about -10.7% for *m*=3 and -16.2% for *m*=5. JM method, LB method and Low-2014 method always provide positive errors with a maximum overestimation of 25.94% for m=3 by JM method.

Table 6 Error of fatigue damage by different methods for m=3 and m=5 for K-joint

		JM	LB	Low-2014	The present method	SM	BT	DK	RFC
m=3	ρ	0.980	0.909	0.865	0.752	0.695	0.766	0.778	0.778
	Error/%	25.94	16.86	11.13	-3.35	-10.7	-1.58	0.03	0.00
m=5	ρ	0.958	0.968	0.895	0.730	0.664	0.751	0.754	0.793
	Error/%	20.79	22.12	12.79	-7.93	-16.2	-5.32	-4.87	0.00

7 Conclusions

This paper studied fatigue damage of offshore wind turbine under combined wind and wave. Dynamic analysis is carried out based on Bladed and ANSYS. Combined stress spectra of X-joints and K-joints are obtained. Finally fatigue damage is

estimated with spectral methods. The main conclusions drawn from the study are as follows:

(1) The proposed half coupling model considers the effect of aerodynamic and structural damping, achieves the separation of turbine system and support structure, avoids the complex modelling process and time-consuming fully coupling analysis. Numerical simulations demonstrate the half coupling model can not only provide accurate fatigue life prediction but also give numerical efficiency and rapid computational speed.

(2) Based on the half coupling model, a half integrated analysis tool combining Bladed and ANSYS is proposed, which can finish fatigue damage assessment of offshore wind turbine under combined wind and wave well. The half integrated analysis tool can be recommended in engineering design of offshore wind turbine.

(3) A linearized Morison equation is developed and achieved in ANSYS for wave spectral analysis.

(4) Among the fatigue damage model mentioned in this paper, it can be conclude that a recently developed spectral combination rule based on HM method is very simple and can give accurate results because only several spectral parameters are needed.

In addition, the paper gives some advantages and disadvantages of the proposed model. The major advantages of the proposed half coupling model are:

- its efficiency in engineering practice for time and computer usage, which makes it

possible to carry out repeated iterative parameter or design variations with a huge potential for design optimization and cost reduction.

- It would be advantageous to use a simplified half coupling model in an early design stage and for parametric studies. It is a promising approach for fatigue assessment of floating OWTs under multiple random loads.

The major disadvantages of the proposed half coupling model are:

- It is not suitable for certification calculations at the end of the design process.

- The calculation can't be performed with the need for a complete wind turbine simulation program.

Acknowledgements

This paper was supported by the National Natural Science Foundation of China (Grant No. 52001144), the Natural Science Foundation of Jiangsu Province (Grant No. BK20190962, BK20211342), the Science and Technology Research Program of Chongqing Municipal Education Commission of China (Grant No. KJQN201900743) and general Program of Natural Science Foundation of Chongqing Municipal of China (Grant No. cstc2019jcyj-msxmX0619).

Reference

[1] GWEC, Global Wind Report 2019, Global Wind Energy Council, Brussels, 2020

[2] Lee J, Zhao F. Global Wind Report 2021, Global Wind Energy Council (GWEC),Brussels, Belgium.

[3] Ferčák O, Bossuyt J, Ali N, Cal RB. Decoupling wind-wave-wake interactions in

a fixed-bottom offshore wind turbine. Applied Energy, 2022; 309: 118358.

[4] Inge Lotsberg. Fatigue design of marine structures. Cambridge University Press, 2016.

[5] Dong WB, Moan T, Gao Z. Long-term fatigue analysis of multi-planar tubular joints for jacket-type offshore wind turbine in time domain. Engineering Structures 2011; 33: 2002-2014.

[6] J.V. Temple, Design of Support Structures for Offshore Wind Turbines, 2006, ISBN 90-76468-11-7 doctoral thesis at delft technical university.

[7] Koukoura C, Brown C, Natarajan A, et al. Cross-wind fatigue analysis of a full scale offshore wind turbine in the case of wind–wave misalignment. Engineering Structures 2016; 120:147-157.

[8] Marino E, Giusti A, Manuel L. Offshore wind turbine fatigue loads: The influence of alternative wave modeling for different turbulent and mean winds. Renewable Energy 2017; 102:157-169.

[9] Rezaei R, Fromme P, Duffour P. Fatigue life sensitivity of monopile-supported offshore wind turbines to damping. Renewable Energy 2018; 123:450-459.

[10] Li H, Hu Z, Wang J, et al. Short-term fatigue analysis for tower base of a spar-type wind turbine under stochastic wind-wave loads. International Journal of Naval Architecture & Ocean Engineering 2017; 10:9-20.

[11] Kvittem M I, Moan T. Time domain analysis procedures for fatigue assessment of a semi-submersible wind turbine. Marine Structures 2015; 40:38-59.

[12] Yang Y, Bashir M, Wang J. Wind-wave coupling effects on the fatigue damage of

tendons for a 10 MW multi-body floating wind turbine. Ocean Engineering, 2020; 217: 107909

[13] Agarwal P, Manuel L. Incorporating irregular nonlinear waves in coupled simulation and reliability studies of offshore wind turbines. Applied Ocean Research 2011; 33: 215-27.

[14] Yeter B, Garbatov Y, Soares CG. Fatigue damage assessment of fixed offshore wind turbine tripod support structures. Engineering Structures 2015; 101: 518-528.

[15] Kvittem MI, Moan T. Frequency versus time domain fatigue analysis of a semi-submersible wind turbine tower. Proceedings of the 33rd international conference on ocean, offshore and arctic engineering, 2014.

[16] Ormberg, H., Bachynski, EE. Global analysis of floating wind turbines: Code development, model sensitivity and benchmark study. In Proceedings of the 22nd International Ocean and Polar Engineering Conference, 2012.

[17] Kvittem, MI., Bachynski, EE., Moan, T. Effects of hydrodynamic modelling in fully coupled simulations of a semi-submersible wind turbine. Energy Procedia, 2012, 24: 351-362.

[18] Kühn M, Dynamics and design optimisation of offshore wind energy conversion systems, doctoral thesis at delft technical university. Holland; 2001, ISBN 90-76468-07-9.

[19] Chen C, Duffour P, Fromme P, Hua XG. Numerically efficient fatigue life prediction of offshore wind turbines using aerodynamic decoupling. Renewable Energy 2021; 178:1421-1434

[20] Sun C, Jahangiri V. Fatigue damage mitigation of offshore wind turbines under real wind and wave conditions. Engineering Structures 2019; 178:472-483

[21] Yeter B, Garbatov Y, Soares CG. Evaluation of fatigue damage model predictions for fixed offshore wind turbine support structures. International journal of Fatigue 2016; 87:71-80.

[22] Li X, Zhang W. Long-term fatigue damage assessment for a floating offshore wind turbine under realistic environmental conditions. Renewable Energy 2020; 159:570-584.

[23] Lin Z, Cevasco D, Collu M. A methodology to develop reduced-order models to support the operation and maintenance of offshore wind turbines. Applied Energy, 2020; 259: 114228.

[24] Wang SS, Moan T, Nejad AR. A comparative study of fully coupled and de-coupled methods on dynamic behaviour of floating wind turbine drivetrains. Renewable Energy 2021; 179:1618-1635.

[25] Lutes LD, Sarkani S. Stochastic analysis of structural and mechanical vibrations. Englewood Cliffs: Prentice-Hall; 1997.

[26] Vanmarcke, EH. Properties of Spectral Moments with Application to Random Vibration, Jour. Engineering Mechanics Division, ASCE, 1972; EM2: 425-445.

[27] Wirsching P H, Light C L. Fatigue under wide band random stresses. ASCE, J Struct Div 1980; 106(7):1593-1607.

[28] Wöhler A. Versuche uber die Festigkeit der Eisenbahnwagenachsen. Zeitschrift für Bauwesen 1860; 10:160-1.

[29] DNV. Recommended practice, fatigue design of offshore steel structures, DNV-RP-C203, 2010.

[30] Miner, MA. Cumulative Damage in Fatigue, Journal Applied Mechanics 1945, 12.

[31] Lutes LD, Corazao M. Stochastic fatigue damage accumulation. J. Struct. Eng. 1984; 110:2585-2601.

[32] China Classification Society. Classification and construction of offshore fixed platform. Beijing, 1992.

[33] DNV. Design of offshore wind turbine structure. DNV-OS-J101, 2007.

[34] Han CS, Liu K, Ma YL, Qin PJ, Zou T. Multiaxial fatigue assessment of jacket-supported offshore wind turbines considering multiple random correlated loads. Renewable Energy 2021; 169:1252-1264.

[35] Burton T., Wind Energy Handbook, John Wiley & Sons Ltd, England, 2001, ISBN 0-471-48997-2.

[36] Dirlik T. Application of computers in fatigue analysis (Ph.D. thesis). University of Warwick; 1985.

[37] Lutes LD, and Larsen CE. Improved spectral method for variable amplitude fatigue prediction. J. Struct. Div., ASCE, 1990; 116(4): 1149-1164.

[38] Benasciutti D, Tovo R. Spectral methods for lifetime prediction under wide-band stationary random processes. Int J Fatigue 2005; 27:867-877.

[39] Jiao G, Moan T. Probabilistic analysis of fatigue due to Gaussian load processes. Probabilistic Engineering Mechanics 1990; 5(2):76-83.

[40] Low Y M. A method for accurate estimation of the fatigue damage induced by bimodal processes. Probab Eng Mech 2010; 25(1):75-85.

[41] Han CS, Ma YL. A practical method for combination of fatigue damage subjected to low-frequency and high-frequency Gaussian random processes. Applied Ocean Research, 2016; 60:47-60.